

MEMS design and fabrication of an electrostatic vibration-to-electricity energy converter

Yi Chiu · Chung-Ting Kuo · Yu-Shan Chu

Received: 28 June 2006 / Accepted: 20 November 2006 / Published online: 4 January 2007
© Springer-Verlag 2007

Abstract This paper presents a micro electrostatic vibration-to-electricity energy converter based on the micro-electromechanical system. For the 3.3 V supply voltage and 1 cm² chip area constraints, optimal design parameters were found from theoretical calculation and Simulink simulation. In the current design, the output power is 200 $\mu\text{W}/\text{cm}^2$ for the optimal load of 8 M Ω . The device was fabricated in a silicon-on-insulator wafer. Mechanical and electrical measurements were conducted. Residual particles caused shortage of the variable capacitor and the output power could not be measured. Fabrication processes are being refined to remove the back silicon substrate to eliminate residual particles and parasitic capacitance.

1 Introduction

Due to the advance of CMOS VLSI technology, the power consumption of electronic devices has been reduced considerably. The low-power technology enables the development of such applications as wireless sensor networks (Rabaey et al. 2000) or personal health monitoring (Tashiro et al. 2000), where remote or independent power supply is critical for building more compact or longer-lifetime systems. In particular,

energy scavenging from ambient natural sources, such as vibration (Roundy et al. 2002), radioisotope (Lal et al. 2005) and ambient heat (Douseki et al. 2003), is attracting much recent interest as a self-sustainable power source for these applications. Among various approaches, electrostatic vibration-to-electricity conversion using the micro-electromechanical systems (MEMS) technology is chosen in this study due to its compatibility to IC processes and the ubiquity of the energy source in nature.

The output power of a vibration driven energy converter is closely related to the nature of the vibration source, which must be known in order to design the converter and estimate the generated power. The vibration spectra of several household appliances were measured. A typical vibration source has a peak acceleration of about 2.25 m/s² at about 120 Hz, as shown in Fig. 1. These values are used in the following static and dynamic analysis for the design of the converter.

2 Design

A variable capacitor C_v formed by an in-plane gap-closing comb structure is the main component in the energy converter (Roundy et al. 2002; Williams and Yates 1996), as shown in Fig. 2. Figure 3 shows a schematic circuit that can be used to extract the converted energy. The variable capacitor C_v is charged by an external voltage source V_{in} through the switch SW1 when C_v is at its maximum C_{max} . When C_v is charged to V_{in} , SW1 is opened and then the capacitance is changed from C_{max} to C_{min} due to the electrode displacement caused by vibration. In this process, the

DTIP2006

Y. Chiu (✉) · C.-T. Kuo · Y.-S. Chu
Department of Electrical and Control Engineering,
National Chiao Tung University, 1001 Ta Hsueh Road,
Hsinchu 300, Taiwan, ROC
e-mail: yichiu@mail.nctu.edu.tw

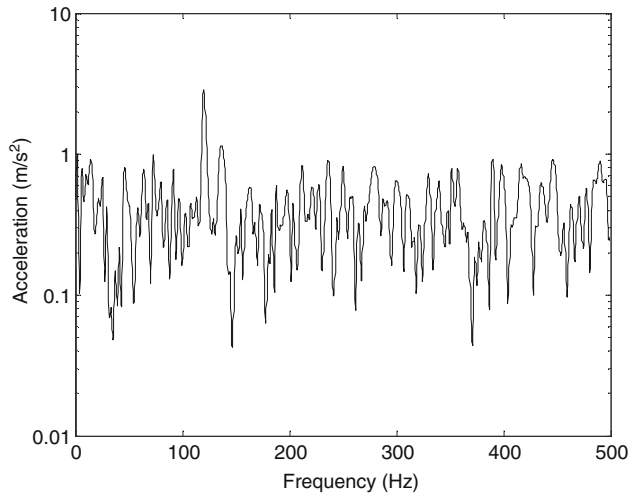


Fig. 1 Typical vibration spectrum of a household appliance

charge Q on the capacitor remains constant (SW1 and SW2 both open). Therefore, the terminal voltage on the capacitor is increased and the vibration energy is converted to the electrostatic energy stored in the capacitor. When the capacitance reaches C_{\min} (V_{\max}), SW2 is closed and the charge on C_v is transferred to a storage capacitor C_{stor} . SW2 is then opened and C_v goes back to C_{\max} , completing one conversion cycle. During the period when SW2 is open, the charge on C_{stor} is discharged by the load resistance R_L with a time constant $\tau = R_L C_{\text{stor}}$ before it is charged again by C_v . In the steady state, the initial and final terminal voltages V_L of the discharge process become constant, as shown in Fig. 4.

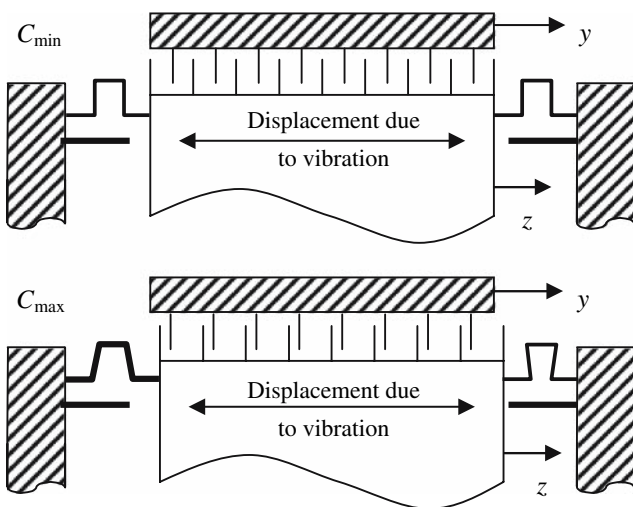


Fig. 2 Variable capacitor schematic

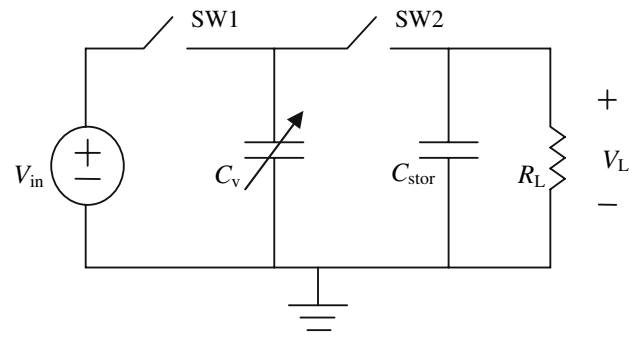


Fig. 3 Operation of the electrostatic energy converter

It can be shown that the steady-state final terminal voltage V_{sat} in the charge-discharge cycle can be expressed as

$$V_{\text{sat}} = \frac{\frac{C_{\max}}{C_{\text{stor}}} V_{\text{in}}}{\left(1 + \frac{C_{\min}}{C_{\text{stor}}}\right) \times \exp(\Delta t / R_L C_{\text{stor}}) - 1}, \quad (1)$$

where $\Delta t =$ conversion cycle time $= 1/2f$ and f is the vibration frequency. When the voltage ripple of the charge-discharge cycle is small, as will be shown subsequently, the output power can be estimated by

$$P_{\text{out}} = \frac{V_{\text{sat}}^2}{R_L}, \quad (2)$$

which is in general proportional to C_{\max}^2 .

In the comb structure, C_{\max} is determined by the minimum finger spacing. In a previous design (Chu et al. 2005), the minimum finger spacing was kept at $0.5 \mu\text{m}$ to prevent shortage of the uninsulated fingers (Fig. 5a). If a dielectric coating is applied to the side walls of the fingers (Fig. 5b), they become insulated and the minimum spacing can be further reduced to increase C_{\max} and P_{out} . In this design, the total capacitance between fingers becomes $C_{\text{dielectric}} \parallel C_{\text{air}} \parallel C_{\text{dielectric}}$. If a layer of 500-Å-thick silicon nitride is used as the dielectric material due to its process compatibility and high dielectric constant ($\epsilon_r \sim 7$), C_{\max} can be

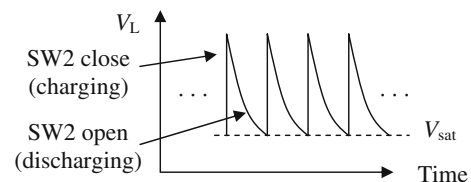


Fig. 4 Output terminal voltage V_L in the steady-state charge-discharge cycle

increased by a factor of four compared to the previous design. It is also noted that the dielectric coating barely increases C_{min} . Therefore, the expected increase of output power will not be affected by the change of C_{min} .

2.1 Static analysis

In Eq. 1, R_L and C_{stor} can be chosen so that the discharge time constant $\tau = R_L C_{stor}$ is much larger than the conversion cycle time Δt . The output voltage ripple in the steady state can therefore be neglected. In this case, V_{sat} can be approximated as

$$V_{sat} = \frac{C_{max} V_{in}}{C_{min} \left(1 + \frac{\Delta t}{R_L C_{min}} + \frac{\Delta t}{R_L C_{stor}} \right)} \quad (3)$$

Usually C_{min} is a small value (in the order of 100 pF). The other circuit components in Eq. 3 can then be chosen so that $C_{stor} \gg C_{min}$ and $R_L C_{min} \ll \Delta t$. The equation can then be simplified as

$$V_{sat} \approx \frac{C_{max} V_{in}}{C_{min} \frac{\Delta t}{R_L C_{min}}} \quad (4)$$

The power output becomes

$$P_{out} \approx \frac{V_{sat}^2}{R_L} \approx \left(\frac{C_{max} V_{in}}{\Delta t} \right)^2 R_L \quad (5)$$

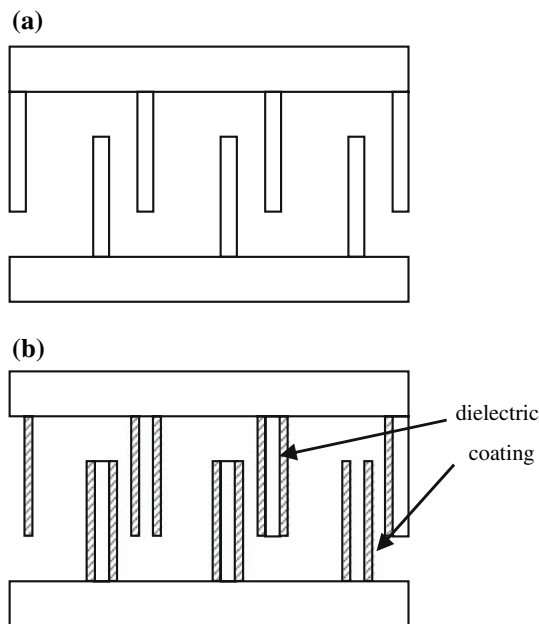


Fig. 5 Variable capacitor at C_{max} position: **a** without coating, **b** with dielectric coating

For a typical low-power sensor node or module, the minimum output power requirement is about 200 μ W. In such a module, a power management circuit is needed to convert the high output voltage to lower ones for various sensing and signal processing units. To be compatible with the power management circuit, the maximum output voltage is limited to about 40 V. With these constraints in Eq. 2, the range of R_L can be found to be $R_L \leq 8 \text{ M}\Omega$. Even though a smaller R_L can be used, C_{max} must then be increased in order to satisfy the voltage and power requirement (Eqs. 4, 5), which in turn have adverse effects in the dynamic behavior of the converter. Therefore, $R_L = 8 \text{ M}\Omega$ and hence $C_{max} = 7 \text{ nF}$ are used in the following calculation.

The output power P_{out} for various C_{stor} and R_L is shown in Fig. 6 for $C_{stor} \gg C_{min}$. It can be seen that the output power does not depend strongly on the storage capacitor C_{stor} when C_{stor} relatively large. Nevertheless, a large C_{stor} will result in long initial charge time when the converter starts to work from a static initial status. Hence, a reasonable C_{stor} of 20 nF is used.

From Eq. 1 and with the values of C_{stor} and R_L obtained from above, input voltage V_{in} of 3.3 V, vibration frequency of 120 Hz, and chip area size of 1 cm^2 , Fig. 7 shows the calculated output saturation voltage and power as a function of the initial finger gap distance for various silicon nitride thickness. The finger thickness, length, and width are 200, 1,200 and 10 μm , respectively (Chu et al. 2005). The dimensions of the fingers are based on the available deep etching process capability. The minimum gap distance is assumed to be 0.1 μm , which is controlled by mechanical stops. It can be seen that with a 500-Å-thick nitride, the initial fin-

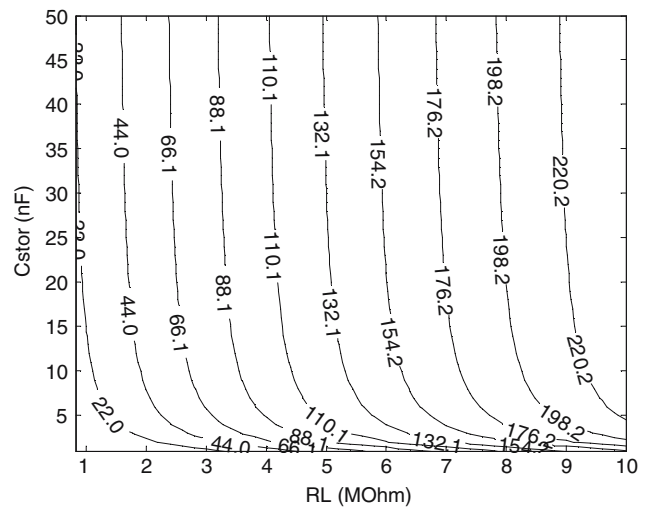


Fig. 6 Contour plot of output power for various R_L and C_{stor}

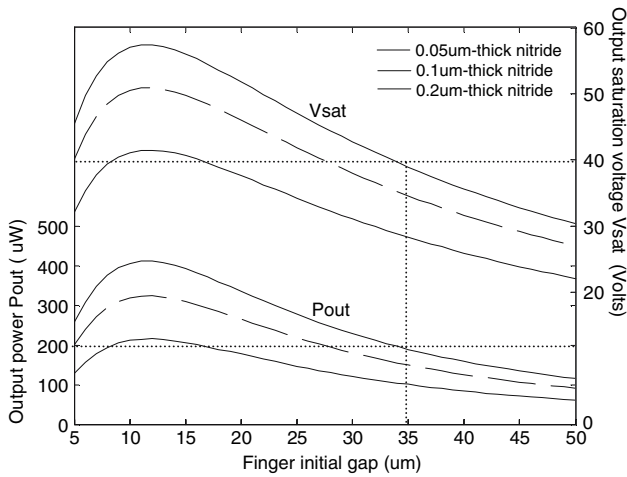


Fig. 7 Output saturation voltage and power versus initial finger gap ($R_L = 8 \text{ M}\Omega$, $C_{\text{stor}} = 20 \text{ nF}$)

ger gap has an optimal value of $35 \mu\text{m}$ for a power output of $200 \mu\text{W}$ and output voltage of 40 V .

2.2 Dynamic analysis

After the dimensions of the variable capacitor are determined from the static analysis, the dynamics of the micro structure is analyzed so that the desired maximum displacement, and hence C_{max} , can be achieved by the target vibration source. The electro-mechanical dynamics of the converter can be modeled as a spring-damper-mass system with the equation of motion,

$$m\ddot{z} + b_e(z) + b_m(z, \dot{z}) + kz = -m\ddot{y}, \tag{6}$$

where y is the displacement of the device frame caused by vibration, z is the displacement of the shuttle mass m with respect to the device frame, $b_m(z, \dot{z})$ is the mechanical damping force representing energy loss caused by the squeezed film effect, and $b_e(z)$ is the electrostatic force acting on the MEMS structure. Notice that the mechanical damping b_m is a function of both the displacement z of the shuttle mass and its velocity \dot{z} (Roundy et al. 2002).

A Simulink model was built to simulate the system dynamic behavior based on Fig. 3 and Eq. 6, as shown in Fig. 8. The charge redistribution box calculates the charging and discharging events when C_v reaches C_{max} or C_{min} . This process represents the power output. Due to the limited shuttle mass that can be achieved in a MEMS process using only silicon, an external attached mass m is considered in order to increase the displacement of the variable capacitor and the energy conversion efficiency.

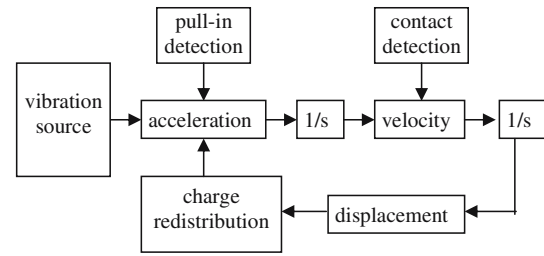


Fig. 8 Dynamic simulation model

For various attached mass, Fig. 9 shows the maximum achievable displacement and required spring constant. It can be seen that a mass of 7.2 g is required to achieve the maximum of $34.8 \mu\text{m}$ according to the static design. The corresponding spring constant, 4.3 kN/m , is used to design the spring structures. With these values, the output voltage simulated by the Simulink model as a function of time is plotted in Fig. 10. The charge-discharge cycles are evident and the saturation voltage V_{sat} is close to the expected value of 40 V . Table 1 summarizes the important device design parameters according to both the static and dynamic analyses.

3 Fabrication

A schematic device layout is shown in Fig. 11. The center hole is used to fix the position of the attached mass. A silicon-on-insulator (SOI) wafer with a $200\text{-}\mu\text{m}$ -thick device layer was used for large capacitance. The oxide layer and the handle wafer are 2 and $500 \mu\text{m}$

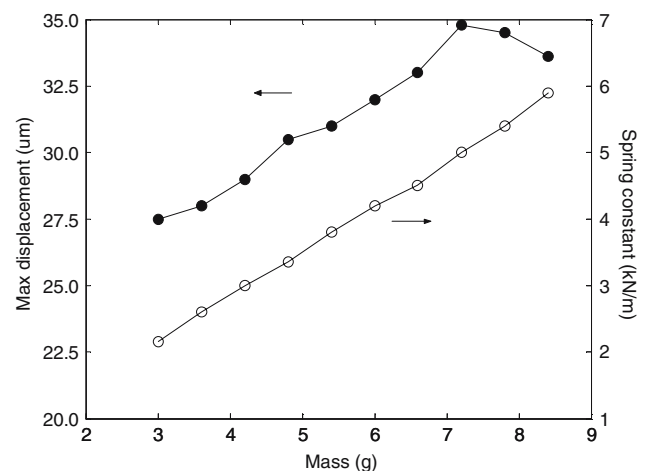


Fig. 9 Maximum displacement and spring constant versus attached mass

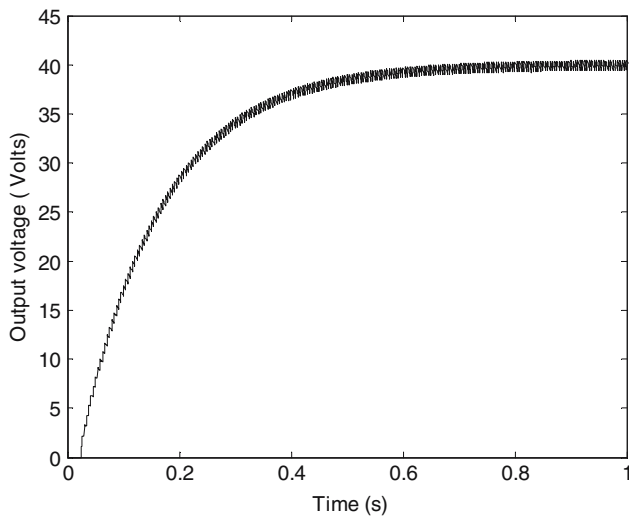


Fig. 10 Output voltage versus time

Table 1 Design parameters of the energy converter

Parameter	Description	
W	Width of shuttle mass	10 mm
L	Length of shuttle mass	8 mm
L_f	Length of finger	1,200 μm
W_f	Width of finger	10 μm
m	Shuttle mass	7.2 g
d	Initial finger gap	35 μm
d_{min}	Minimum finger gap	0.1 μm
C_{stor}	Storage capacitance	20 nF
K	Spring constant	4.3 kN/m
T	Dielectric layer thickness	500 \AA
ϵ_r	Dielectric constant	7 (SiN)
R_L	Load resistance	8 M Ω
V_{sat}	Output voltage	~40 V
P_{out}	Output power	~200 μW

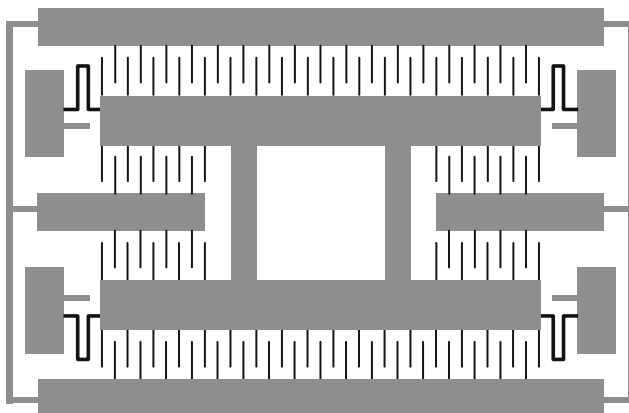


Fig. 11 Device layout schematic

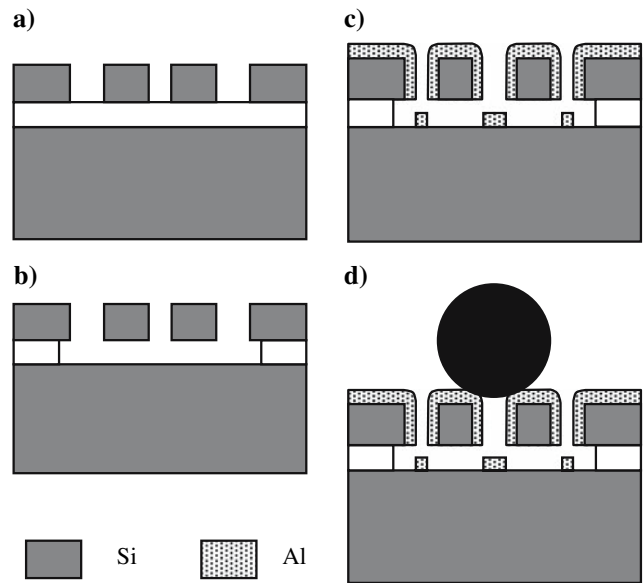


Fig. 12 Fabrication process: **a** define structure by DRIE, **b** etch oxide by HF solution, **c** apply Al by thermal evaporation, and **d** attach external mass

thick, respectively. Figure 12 shows an earlier fabrication process without the dielectric coating. The variable capacitor structure is first defined by deep reactive ion etching (DRIE) (Fig. 12a). After the sacrificial oxide layer is removed using HF solution (Fig. 12b), aluminum is evaporated for electrical contact (Fig. 12c). A steel ball is then attached to the central plate to adjust the resonant frequency to match the vibration source and improve the conversion efficiency (Fig. 12d).

The fabricated first-generation device is shown in Fig. 13 (Chu et al. 2005). The width of the finger was reduced to 6.8 μm due to the variation in photolithography and RIE processes. The deviation will affect the characteristics of the converter such as the resonant frequency, output power, and output voltage.

4 Measurement

4.1 Mechanical measurement

The displacement of the device without the attached mass was measured using a PROWAVE JZK-1 shaker. The measured response is shown in Fig. 14. Since the mass was not attached, the vibration acceleration was increased to 40 m/s^2 for easy observation. The maximum displacement was about 10 μm at 800 Hz, and the quality factor $Q = \omega_0 / \Delta\omega$ was about 10, where ω_0 was the resonant frequency and $\Delta\omega$ was the resonant

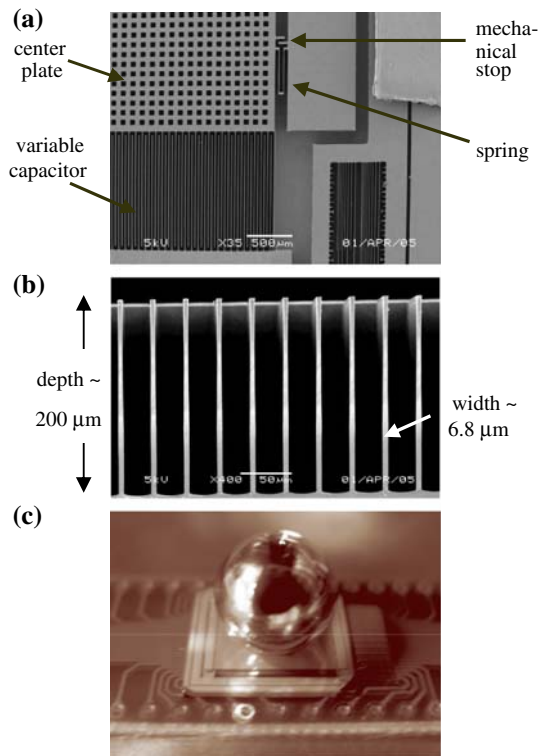


Fig. 13 Fabricated device: **a** top view, **b** cross section of comb fingers, **c** overview of the converter with attached mass

bandwidth shown in Fig. 14. The mass of the center plate was approximately 0.038 g, thus the spring constant can be calculated as $k = \omega_0^2 m = 960$ N/m. The measured spring constant is different from the design mainly due to the reduced spring width as shown in Fig. 13.

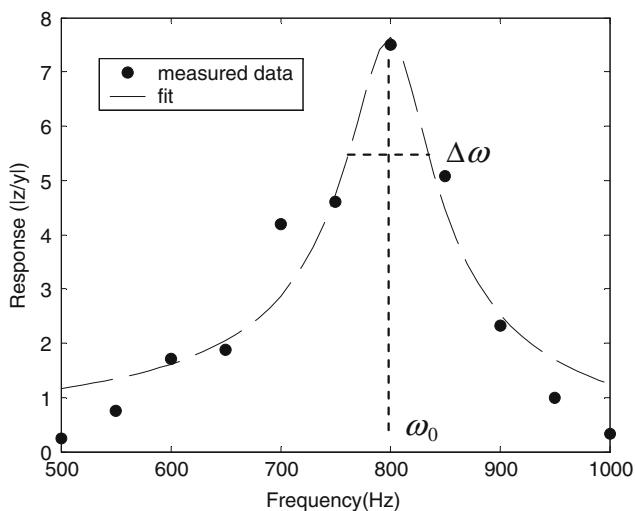


Fig. 14 Frequency response of the device

4.2 Electrical measurement

The electrical measurement was conducted using an INSTRON-LCR-816 LCR meter and a HP-4192A impedance analyzer. The measured capacitance without vibration was about 500 ~ 600 pF, while the calculated capacitance C_{\min} is about 50 pf. The major contribution of the large capacitance is the parasitic capacitance C_{par} between the center plate and the underneath substrate.

In addition to the parasitic capacitance, there was also a parallel parasitic conductance. The measured conductance varied from die to die with an average resistance of 2.5 k Ω . It is suspected to be caused by the residual particles left in the device after the release process. The presence of the parasitic capacitance and conductance had hindered the measurement of output power. New devices are being fabricated with the underneath substrate removed to prevent residual particles and reduce parasitic capacitance.

5 Conclusion

The design and analysis of a micro vibration-to-electricity converter have been presented. The device was fabricated in a SOI wafer. The reduced feature size of the fabricated device resulted in the decrease of spring constants. Mechanical and electrical measurements of the fabricated device were conducted. Impedance measurements showed an unwanted parasitic conductance which resulted in the failure of output power measurement. Improvement of the fabrication processes is being conducted.

Acknowledgment This project was supported in part by the National Science Council, Taiwan, R.O.C, under the grant No. NSC 93-2215-E-009-066. The authors are grateful to the National Center for High-performance Computing, Taiwan, ROC, for computer time and facilities.

References

- Chu YS, Kuo CT, Chiu Y (2005) A MEMS electrostatic vibration-to-electricity energy converter. In: Proceedings of PowerMEMS, pp 49–52
- Douseki T, Yoshida Y, Utsunomiya F, Ito N, Hama N (2003) A batteryless wireless system uses ambient heat with a reversible-power-source compatible CMOS/SOI DC-DC converter. In: Proceedings of the IEEE international solid-state circuits conference, pp 388–389
- Lal A, Duggirala R, Li H (2005) Pervasive power: a radioisotope-powered piezoelectric generator. IEEE Pervasive Comput 04(1):53–61

- Rabaey JM, Ammer MJ, da Silva JL Jr, Patel D, Roundy S (2000) Picoradio supports ad hoc ultra low-power wireless networking. *IEEE Comput Mag* 33:42–48
- Roundy S, Wright PK, Pister KS (2002) Micro-electrostatic vibration-to-electricity converters. In: *Proceedings of 2002 ASME International Mechanical Engineering Congress and Exposition*, pp 393–409
- Tashiro R, Kabei N, Katayama K, Ishizuka Y, Tsuboi F, Tsuchiya K (2000) Development of an electrostatic generator that harnesses the motion of a living body: (use of a resonant phenomenon). *JSME Int J ser C* 43(4):916–922
- Williams CB, Yates RB (1996) Analysis of micro-electric generator for microsystems. *Sensors Actuators A* 52:8–11